Accepted Manuscript

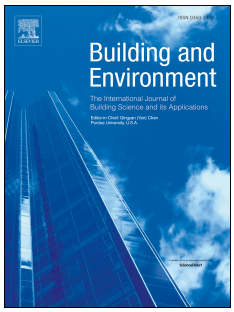

Steady flows in a naturally-ventilated enclosure containing both a distributed and a localised source of buoyancy

J.L. Partridge, P.F. Linden

PII: S0360-1323(17)30376-1

DOI: 10.1016/j.buildenv.2017.08.023

Reference: BAE 5048

To appear in: *Building and Environment*

Received Date: 11 July 2017

Revised Date: 10 August 2017

Accepted Date: 14 August 2017

Please cite this article as: Partridge JL, Linden PF, Steady flows in a naturally-ventilated enclosure containing both a distributed and a localised source of buoyancy, *Building and Environment* (2017), doi: 10.1016/j.buildenv.2017.08.023.

This is a PDF file of an unedited manuscript that has been accepted for publication. As a service to our customers we are providing this early version of the manuscript. The manuscript will undergo copyediting, typesetting, and review of the resulting proof before it is published in its final form. Please note that during the production process errors may be discovered which could affect the content, and all legal disclaimers that apply to the journal pertain.

ACCEPTED MANUSCRIPT

Steady flows in a naturally-ventilated enclosure containing both a distributed and a localised source of buoyancy

J. L. Partridge[a] P. F. Linden[a]

[a]Department of Applied Mathematics and Theoretical Physics, University of Cambridge, Cambridge, CB3 0WA, UK

Corresponding author: J. L. Partridge email:jlp56@cam.ac.uk
tel: +441223 764064

Abstract

We consider the flows and stratification established in a naturally-ventilated enclosure containing both localised and distributed sources of buoyancy. In this study, both the localised and distributed sources originate from the same horizontal plane, with both adding buoyancy to the enclosure, i.e. representing a point source of heat and a horizontally distributed source of heat at the base of a room. An important parameter controlling the transient and steady states of the enclosure is the ratio of the source buoyancy fluxes $\psi = \frac{B_D}{B_L}$, with B_D and B_L the source buoyancy flux of the distributed and localised source, respectively. We examine the role of entrainment between the layers, due to turbulent mixing, and construct a mathematical model to predict the stratification within the room for a range of ψ. We also show that for large ψ and opening areas the two-layer nature of the flow breaks down and there is a short circuit that allows the incoming air to escape through the upper opening without interacting with the full volume of the space. The validity of this model and its break down as predicted by a critical Richardson number are verified against small-scale experiments and the consequences for real-world buildings are discussed.

Keywords: natural ventilation; plume; heated floor; small-scale experiments;

1 Introduction

Natural ventilation harnesses the natural conditions of an environment to drive a ventilation flow (i.e. the flow between an indoor enclosure and the exterior ambient) and establish a thermal stratification within the enclosure. On the other hand, mechanical ventilation uses energy directly to impose a desired ventilation

ACCEPTED MANUSCRIPT

flow rate and thermal stratification. Mechanical ventilation has the advantage that buildings can be designed with little constraint on how the building will perform thermally. For example, buildings with large glazed facades can be air conditioned to give comfortable interior conditions. Unfortunately, heating, ventilation and air conditioning (HVAC) uses significant amounts of energy and produces greenhouse gas (GHG) emissions. Mechanical ventilation accounts for approximately half of the built environment energy consumption, which itself accounts for $20-40\%$ of total energy consumption in the developed world (Pérez-Lombard et al., 2008). Given the urgent need to reduced energy consumption and GHG emissions, it is desirable to use naturally-ventilated buildings where possible. However, as a naturally-ventilated building relies solely on the natural conditions of the environment, smart design of such buildings is required to guarantee thermally comfortable, well-ventilated buildings. The adequate design of naturally-ventilated buildings relies on an understanding of the underlying fluid mechanics that control the flow and stratification within the enclosure (Linden, 1999). This makes mathematical models powerful tools in the design of naturally-ventilated buildings.

There has been a great deal of work in this area, especially in the last three decades, with much of the understanding coming from small-scale experimental studies in conjunction with the development of theoretical models starting with the work of Linden et al. (1990). Linden et al. (1990) conducted a series of small-scale experimental models to verify a mathematical model that predicted the steady-state ventilation flow rate and thermal stratification within an enclosure containing a single, or multiple non-interacting localised sources of buoyancy (heat). Localised sources are good models for the flow produced by people, equipment or lighting. Localised sources generate turbulent plumes that transport buoyancy throughout the space and can be solely parameterised, in the idealised case of a point source, by a buoyancy flux B_L. For a source with a heat flux W_L, B_L can be determined from

$$B_L = \frac{g\beta W_L}{\rho C_p}, \tag{1}$$

where g is gravitational acceleration, β is the thermal expansion coefficient, ρ is the density and C_p is the specific heat at constant pressure.

Further work has investigated other fundamental natural-ventilation flows including: the transients of naturally-ventilated enclosures containing localised (Kaye and Hunt, 2004) or a distributed source, e.g. representing a sun patch on the floor (Fitzgerald and Woods, 2007); wind-driven or wind-assisted natural ventilation (e.g. Hunt and Linden (2001) and Coomaraswamy and Caulfield (2011)); flows within complex enclosures, e.g. atria (Holford and Hunt, 2003); the role of thermal mass within the enclosure (Holford and Woods, 2007); and the role of radiative heating (e.g. Lane-Serff and Sandbach (2012) and Menchaca-Brandan et al. (2017)). However, to date the interaction between localised and distributed sources in naturally-ventilated enclosures remains unstudied. Distributed sources are very common, such as a floor being heated from a space below or a patch of floor heated by solar gains through a window.

ACCEPTED MANUSCRIPT

Furthermore, due to the prevalence of both types of buoyancy source in a building, the interaction of the flow generated by them and the subsequent effect on the ventilation and stratification within a building needs to be understood and modelled. Moreover, the need for reduced mathematical models of such flows needed to assist the design of naturally-ventilated buildings due to the computational cost of computational fluid dynamics (CFD).

Wells et al. (1999) examined the competition between a localised and distributed source of buoyancy in an *unventilated* enclosure. They considered the case of two buoyancy sources located in the bottom boundary, with both providing a positive flux of buoyancy into the space, i.e. in a building both sources would be heating the space. In such a scenario, they found that the enclosure could either be completely stratified, completely mixed, or have both a stratified and mixed region depending on the ratio of the buoyancy fluxes $\psi = \frac{B_D}{B_L}$, where B_D is the buoyancy flux from the distributed source and B_L is the buoyancy flux of the localised source. For $0 < \psi < 1$ the classic filling box mechanism stratified the upper region of the enclosure and the distributed source was only able to mix the lower region. However, if $\psi > 1$ the convective motion from the distributed source was too strong compared to the stratification formed by the filling box flow, and the fluid in the enclosure became, to a good approximation, well mixed.

For the ventilated case, Hunt et al. (2001b) conducted some preliminary experiments in the set-up we seek to model here. As in the unventilated case, the dynamics depends on the ratio of buoyancy fluxes ψ. There are two limiting cases: when $\psi = \infty$ the space becomes well mixed, driven by a distributed source of buoyancy alone, whereas in the opposite limit, $\psi = 0$, the space becomes stratified with a two-layer stratification (Linden et al., 1990). Empirically, a critical value ψ_c corresponding to the transition between these possible states was found: for $\psi < \psi_c$ the space can maintain a stratification, and for $\psi > \psi_c$ the space becomes well mixed. The experiments of Hunt et al. (2001b) suggested $\psi_c \simeq 6$ which was found to be independent of the effective opening area

$$A^* = \frac{2c_b c_t a_b a_t}{\sqrt{2\left(c_b^2 a_b^2 + c_t^2 a_t^2\right)}}, \tag{2}$$

where a_t and a_b are the area of the upper and lower openings, respectively and c_t, c_b are coefficients accounting for dissipation and the contraction of the flow through the sharp upper and lower openings (Linden, 1999).

Similar steady states, stratified and well mixed, are also found when the ventilation flow rate is imposed, as is the case of a mechanically ventilated space. Chenvidyakarn and Woods (2008) constructed a steady-state model for such a system and validated their theory with small-scale experiments. They found that the stratification within the room was set by the ratio of the buoyancy fluxes ψ and also the imposed ventilation rate. For small ψ or low ventilation rates there was a two-layer stratification within the space but for large ψ or high ventilation rates the space became approximately well mixed, as if driven by a distributed heat source alone with buoyancy flux $B_D + B_L$.

ACCEPTED MANUSCRIPT

In this paper we extend these studies by examining the steady states of a naturally-ventilated enclosure with both a distributed and a localised heat source originating from the bottom boundary of the enclosure, where the ventilation flow rate is dependent on the effective opening area A^*.

The theoretical model is discussed in §2. Experiments are described §3 and compared with the theoretical model in §4. The breakdown of the simplified model is discussed in §5. An application of the theory is detailed in §6. Finally, conclusions are given in §7.

2 Problem description

We consider the steady states of buoyancy-driven flow in a ventilated enclosure containing both a localised and distributed source of buoyancy originating from the lower boundary. The enclosure is a rectangular box with height H, cross-sectional area S and vertical openings at the top and bottom of the side walls, of areas a_t and a_b, respectively. The openings connect the enclosure to an exterior ambient environment of constant density ρ_a. The localised source has a constant buoyancy flux B_L and is located on the lower boundary along with the horizontally distributed source, covering the full extent of the boundary, that has a constant and spatially uniform buoyancy flux B_D.

First we consider the flows and stratification of an enclosure containing only a localised source of buoyancy. The flow from the localised source will rise through the enclosure as a buoyant plume, increasing in volume flux while losing buoyancy due to entrainment of ambient fluid. The plume spreads radially when it reaches the upper boundary of the enclosure and forms a horizontal front between the buoyant and ambient fluid that descends through the enclosure. It has been previously shown that, for an initially unstratified ambient and plume with constant buoyancy flux B_L, the enclosure will reach a steady state with a stable two-layer stratification consisting of two layers with uniform, but different, temperatures and with depths that are independent of B_L (Linden et al., 1990).

On the other hand, when a ventilated enclosure contains only a distributed source of constant buoyancy flux B_D at high Rayleigh number the convection is turbulent and, to a first approximation, a well-mixed steady state is reached (Gladstone and Woods, 2001). The steady-state buoyancy of the enclosure can be calculated by determining the ventilation flow rate and balancing the buoyancy flux into and out of the enclosure. The flow rate out of the enclosure, when in a well-mixed steady state, is given by

$$Q_v = A^* \sqrt{g'_m H}, \tag{3}$$

where $g'_m = g\frac{\rho_m - \rho_a}{\rho_a}$ is the reduced gravity of the fluid in the well-mixed enclosure, a measure of how buoyant the fluid is. Therefore, the buoyancy flux (the flux of g') out of the space is given by $g'_m Q_v$. Balancing this buoyancy flux out

ACCEPTED MANUSCRIPT

with the buoyancy flux supplied by the distributed source B_D yields

$$g'_m = \frac{B_D^{2/3}}{(A^{*2}H)^{1/3}}. \tag{4}$$

These two cases represent limits to the problem considered here. To reiterate, the parameter describing the relative and competing effects of the localised and distributed sources is the ratio of the buoyancy fluxes

$$\psi = \frac{B_D}{B_L}, \tag{5}$$

and the limiting cases correspond to $\psi = 0$ (localised source only) and $\psi = \infty$ (distributed source only).

We hypothesise, based on experimental evidence (Hunt et al., 2001b), that for $\psi < \psi_c$ the enclosure will exhibit a stable two-layer stratification but for $\psi > \psi_c$ there will be no apparent stratification and the space will become well mixed. The two possible regimes, set by the value of ψ, are shown in Figure 1. One notable difference between the two-layer stratification obtained here and the stratification obtained when a space contains only a localised source is the non-zero buoyancy of the lower layer, which is now heated by the distributed source, i.e. $\rho_l < \rho_a$. Further, we expect that the convection driven by the heated floor in the lower layer will cause entrainment of upper layer fluid into the lower layer. Due to the orientation of the openings, we also anticipate a large-scale circulation within the room when it is well mixed, as shown in Figure 1. The importance of this circulation will be revisited in §5. We now seek to derive a simple steady-state model to capture the dependence of ψ on the steady-state flow rates and distribution of buoyancy within the enclosure.

2.1 Theoretical model

We develop a steady-state model by balancing the volume flow rates and buoyancy within the enclosure. In steady state conservation of volume requires

$$Q_v = Q_p - Q_e, \tag{6}$$

where Q_p is the volume flux in the plume at the interface height h, Q_e is the volume flux of fluid entrained across the interface, and Q_v is the ventilation flow rate out of the enclosure, which is driven by the pressure difference between the interior and exterior. Following Linden et al. (1990), assuming, because of the slow flow in the interior, the pressure is hydrostatic and also assuming the two layers are well mixed we obtain

$$Q_v = A^* \left(\int_0^H g' \mathrm{d}z \right)^{1/2} = A^* \sqrt{g'_u (H-h) + g'_l h}. \tag{7}$$

ACCEPTED MANUSCRIPT

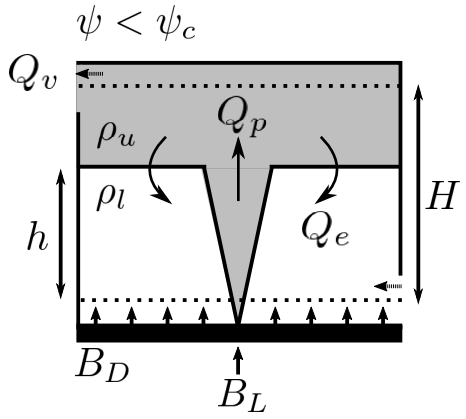

Figure 1: Schematic of the steady state: two-layer stratification for $\psi < \psi_c$, and well-mixed interior for $\psi > \psi_c$. The interface height h is relative to the middle of the lower opening, h_o is the half-height of the opening and z_v is the virtual origin correction.

It is worth noting that the ventilation flow rate Q_v now also depends on the buoyancy of the lower layer g'_l as well as that of the upper layer g'_u. The plume volume flux can be obtained from the plume theory of Morton et al. (1956)

$$Q_p = C {B_L}^{1/3} h^{5/3}, \tag{8}$$

where $C = \frac{6}{5}\alpha \left(\frac{9}{10}\alpha\right)^{1/3} \pi^{2/3}$ is a constant that contains the entrainment coefficient α. A value of $C = 0.17$ (cf. Chenvidyakarn and Woods (2008)) was used in the theoretical modelling of this paper.

The new and critical aspect of this problem is the possibility of entrainment of upper layer fluid across the interface by the turbulence generated by the convection driven by the heated floor. We expect that when the turbulent velocities in the lower layer are higher than those in the upper layer there will be a net volume flux from the upper layer into the lower layer. This turbulent entrainment can not be calculated explicitly and needs to be represented in an approximate manner through a parameterisation based on the average properties of the system. There have been a number of studies which examine the evolution of a density interface when heated from below, for example, Deardorff et al. (1969) and Heidt (1977). Such studies observe mixing across the interface caused by turbulent eddies entraining fluid as they impinge on the interface. A simple way to model this entrainment is to assume the buoyancy flux across the interface is proportional to the buoyancy flux from the floor, i.e. $B_e = \phi B_D$, with ϕ some empirical constant typically in the range $0.05 - 0.2$ (Heidt, 1977). Using this parameterisation the entrainment volume flux is given by

$$Q_e = \frac{\phi B_D}{\Delta g'}, \tag{9}$$

ACCEPTED MANUSCRIPT

where $\Delta g' = {g'}_u - {g'}_l$ is the buoyancy jump across the interface. Representing the entrainment across the interface in this manner closes the system. All that remains is to balance the buoyancy fluxes through the enclosure to determine relations for the buoyancy of the upper and lower layers.

In the case of a steady two-layer stratification, where both layers are well mixed, matching the buoyancy fluxes into and out of the enclosure gives

$$ {g'}_u Q_v = B_L + B_D. \tag{10}$$

Similarly, for the lower layer

$$ B_D + B_e = B_D \left(1 + \frac{{g'}_u \phi}{{g'}_u - {g'}_l}\right) = {g'}_l Q_p, \tag{11}$$

making use of (9).

We now have a system of three equations (6), (10) and (11) to solve for the three unknowns: h, ${g'}_u$ and ${g'}_l$. We first define dimensionless variables:

$$ \zeta = \frac{h}{H} \quad \hat{g}_u = \frac{{g'}_u}{g'_H} \quad \hat{g}_l = \frac{{g'}_l}{{g'}_H} \quad \psi = \frac{B_D}{B_L} \quad \beta = \frac{A^*}{C^{3/2} H^2}, \tag{12}$$

where ${g_H}' = C^{-1} {B_L}^{2/3} H^{-5/3}$ is the reduced gravity of the plume at height H. Substituting (12) into (6), (10), (11) and solving we obtain

$$ \hat{g}_l = \frac{\psi(1+\phi)}{\zeta^{5/3}(1-\phi\psi)} \quad \text{and} \quad \hat{g}_u = \frac{\psi + 1}{\zeta^{5/3}(1-\phi\psi)}, \tag{13}$$

for the buoyancy of the upper and lower layers and an implicit equation for the interface height ζ in the form

$$ \beta = \left(\frac{\zeta^5 (1-\phi\psi)^3}{1 - \zeta + \psi(1+\phi\zeta)}\right)^{1/2}. \tag{14}$$

It is worth noting that, as in the case of a localised source alone, the interface height is not dependent on the magnitude of the buoyancy fluxes present within the system, and it cannot be on dimensional grounds. However, it is now dependent on the ratio of the fluxes ψ.

Setting $\psi = 0$ we find

$$ \hat{g}_l = 0 \qquad \hat{g}_u = \frac{1}{\zeta^{5/3}}, \tag{15}$$

$$ \beta = \left(\frac{\zeta^5}{1-\zeta}\right)^{1/2}, \tag{16}$$

which correspond to the solutions found for an enclosure containing a single localised source (Linden et al., 1990).

We can also investigate when the stratified model breaks down for large ψ. If turbulent entrainment across the layers is active, $\phi > 0$, one limit is $\psi = \frac{1}{\phi}$.

ACCEPTED MANUSCRIPT

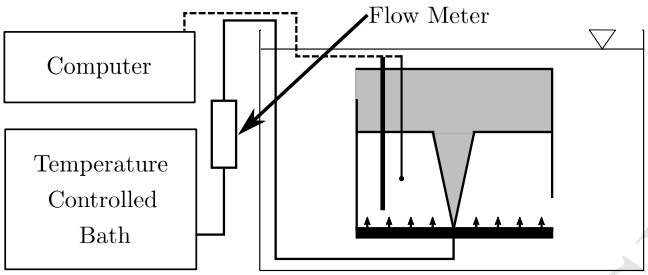

Figure 2: Schematic of the laboratory set-up.

For $0.05 \leq \phi \leq 0.2$ this would result in $5 \leq \psi \leq 20$. In the absence of turbulent entrainment between the layers, $\phi = 0$, we can set $\zeta = 1$ in (14) and find

$$\psi = \frac{1}{\beta^2} \tag{17}$$

which gives a limit on the value of ψ where stratification can persist in the model in the absence of turbulent entrainment between the layers.

The theoretical model given in (13)-(14) is now compared with experimental data.

3 Experimental Set-up

A schematic of the experimental set-up is given in Figure 2. The apparatus consisted of a large ambient reservoir, height 0.8 m and cross sectional area 2.4 m^2. Submersed within the ambient reservoir was a smaller tank, height 34 cm and cross sectional area 1760 cm^2. The small tank represented a model room and had openings located in two opposing vertical walls that connected the interior of the small tank to the large external reservoir. The openings were split into high and low level openings to permit displacement ventilation. The area of each set of openings could be varied from 0 cm^2 to a maximal opening area of 160 cm^2 with increments of 4 cm^2. The opening area was varied by plugging some of the openings with plastic spacers. The spacers had to slip past an O-ring seal and provided a tight fit.

The small tank was highly adjustable and designed by Prof. Gary Hunt, Dr Joanne Holford and David Page-Croft to allow distributed heating at the boundaries (G. R. Hunt, personal communication, March, 2015). The tanks boundaries were a composite construction, similar to double glazing, with a 1 cm air gap sandwiched between two 1.25 cm acrylic panels, this construction was designed to minimise unwanted heat loss through the fabric of the enclosure. The tank was previously used, without the heated floor, in the study of Partridge and Linden (2013) to replicate the results of higher Péclet number, saline plumes where the role of heat loss through the enclosure was found to be negligible. For

ACCEPTED MANUSCRIPT

the present study the floor panel was replaced with a distributed heat source of constant buoyancy flux keeping all other boundaries insulated. A constant buoyancy flux distributed source was established by attaching a heater mat to a 0.4 cm thick brass plate that formed the lower boundary. Polystyrene was sandwiched between the heater mat and outer acrylic sheet to minimise any losses through the base of the enclosure. A controllable power supply provided power to the heater mat; the buoyancy flux of the distributed source was then determined from

$$B_D = \frac{g\beta_e H_f}{\rho C_p}, \tag{18}$$

where β_e is the thermal expansion coefficient which is assumed constant $\beta_e = 2.07 \cdot 10^{-4}$ K^{-1} given the small temperature range between the distributed heat source and the lower layer, $C_p = 4.183$ kJ kg^{-1} K^{-1} is the specific heat capacity also assumed constant, and H_f the heat flux of the source. The heat flux H_f was calculated from the power applied to the mat and was verified by sealing the tank and monitoring the temperature increase within the enclosure by a vertical array of equispaced thermocouples (discussed in §3.2). An alternative method of verifying the buoyancy flux of the distributed source was to use (4) to model the well-mixed reduced gravity of the interior as in Figure 3. The agreement confirms the minimal heat loss through the lower boundary and consequently the value of B_D achieved. The small standard error between thermocouples, which was less than the size of the data points, validates the assumption that the interior is well mixed as found by previous experimental studies (Gladstone and Woods (2001) and Kaye and Hunt (2007), for example). The preliminary experiments with the distributed source alone also revealed that a large circulation is established within the enclosure, as illustrated in Figure 1. The circulation appeared to be established by the flow through the vertical inlet adjacent to the distributed source. The role this circulation plays on the steady states of the enclosure when driven by both the localised and distributed sources is discussed in §4.

3.1 Establishing a plume

The localised source of buoyancy was supplied via a turbulent plume nozzle based on the design of Dr Paul Cooper. The nozzle is designed to establish fully developed turbulence close to the source, typically within 1-2 source diameters D_s, with $D_s << H$ the interior height of the box (see Hunt and Linden (2001) for details).

Fluid was supplied to the plume nozzle by a Grant Optima$^{\text{TM}}$ LTC4 temperature controlled bath with built-in pump. The temperature of the bath, when working with fresh water, could be set between $4 - 80\,^{\circ}$C with a resolution of $0.1\,^{\circ}$C. For the experiments herein, the typical temperature difference relative to the ambient ΔT of the fluid at the source was $\Delta T = 15 - 30\,^{\circ}$C resulting in a source buoyancy flux $B_L \sim 6 - 15$ cm^4 s^{-3}. The flow rate of the built-in pump was far too high for the experiments detailed here (~ 300 cm^{3}s^{-1}), so the flow rate was controlled via a valve and monitored using an in-line flow meter.

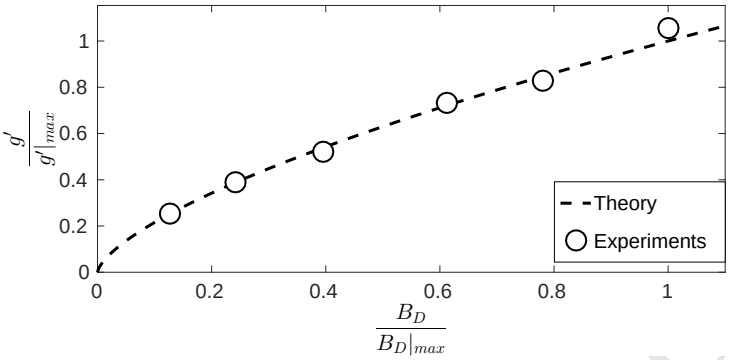

Figure 3: Experimental and theoretical steady-state reduced gravity of an enclosure containing only a distributed source of buoyancy. $\hat{B_D}$ is the maximum buoyancy flux achievable with the heater mat and g'_{max} is the corresponding steady-state reduced gravity. Experimental values correspond to the mean of the eight fixed thermocouples, representing a spatial average over the height of the tank. The standard error was small, the size of the data points, and justifies the well-mixed assumption.

A simple float style flow meter was used for all the experiments. The plume source flow rate Q_s used in the experiments was in the range $1-2$ cm^{3}s^{-1} and was $< 5\%$ of the ventilation flow rate Q_v and for most experiments $1-2\%$. A virtual origin correction was made to the experimental data such that any theoretical model could consider the plume as a source of buoyancy flux only (Hunt and Kaye, 2001).

The temperature of the supply was monitored via a T-type thermocouple just below the plume nozzle. This was done for two reasons. First, to be able to record the supply temperature, as there were losses from the heater bath to the source. Second, to monitor the supply temperature to check that it remained constant throughout the experiment. Typically the plume source had a variation in temperature of 1% that resulted in negligible fluctuations in the buoyancy flux of the plume. The hot water bath was resupplied by a gravity feed from the ambient reservoir. This method of establishing a plume was chosen over the alternative of an electrically heated element as, given the fluid used, the power density of such an element would result in localised boiling at the source.

The experimental plumes for this study were forced plumes to allow a large enough volume flux at the source Q_s such that the flow was turbulent close to the plume nozzle. However, this should have minimal impact on the experimental results as the lengthscale over which the plume is noticebly forced is given by the jet length L_j where

$$L_j = 2^{-3/2}\alpha^{-1/2}\frac{M_s^{3/4}}{B_L^{1/2}}, \tag{19}$$

ACCEPTED MANUSCRIPT

as in Hunt and Kaye (2001) with M_s the momentum flux of the plume at the source. In all of the experiments the jet length was kept small, $L_j < 0.1H$, to minimise the impact of forcing on the ventilation flow (Hunt et al., 2001a), and a virtual origin correction was used to match the plumes in the laboratory to the idealised point source assumed in the theory.

3.2 Temperature measurements

The temperatures, and hence the reduced gravities, of the interior of the small tank were monitored in two ways using T-type thermocouples. The first was via an array of eight thermocouples extending over the height of the tank. The thermocouples were located at heights above the floor $\frac{z}{H} = 0.05$, 0.17, 0.28, 0.4, 0.52, 0.63, 0.75, 0.86. The second method was a traversing thermocouple that travelled the height of the tank. These arrangements allowed temperatures to be recorded at different fixed heights throughout the experiments and continuous temperature profiles to be measured over most of the height of the enclosure, between $0 \leq \frac{z}{H} \leq 0.82$.

Temperatures were recorded using National Instruments equipment. The array was recorded using a NI-9213 data logger, capable of recording 16 thermocouples at 5 Hz, and data were logged using LabView SignalExpress. The traverse mechanism itself was driven via a NI-6008 controller, to send pulses to a stepper motor, which was also controlled via LabView. The stepper motor was pulsed at 125 Hz, and took approximately three minutes to traverse 28 cm through the tank. This traverse speed was chosen to minimize the lag associated with the time response of the thermocouple. The traverse speed was comparable to the filling ($T_f = \frac{S}{CB_L{}^{1/3}H^{2/3}}$) and draining time scale ($T_d = \frac{SH^{1/2}}{A^* g'^{1/2}}$) associated with the experiments but profiles were only ever taken when the system had a reached a steady state ($t > 4T_f$), and the temperature change with time was negligible. The thermocouples were calibrated in LabView by placing them in a hot water bath over an appropriate temperature range. With careful calibration, accuracies to within $\pm 0.1\,^{\circ}\mathrm{C}$ were obtained.

3.3 Loss coefficients

In all experiments there will be energy loss due to dissipation and contraction as the fluid passes through the openings. Following Linden et al. (1990), these losses can be included with loss coefficients c_t and c_b to take into account the contraction at the top and bottom opening, respectively. Typically, the loss coefficients are both given the value 0.6 corresponding to sharp openings but, for large buoyancy differences they have been shown to be dependent on the buoyancy difference, between the fluid in the enclosure and the ambient fluid (Holford and Hunt, 2001). Calibration experiments were conducted for the current set-up, by filling the tank with a buoyant solution and tracking the interface of the subsequent draining flow through the openings, and good agreement was found using the commonly used value of $c_t = c_b = 0.6$. The insensitivity of the

ACCEPTED MANUSCRIPT

loss coefficients in the current set-up is likely due to the relatively small buoyancy differences associated with these thermal plume experiments compared to those driven by salinity.

3.4 Visualisation

Experiments were also visualised using the shadowgraph technique. A slide projector illuminated a section (approximately 1 m^2) of the large ambient reservoir that contained the smaller tank. On the front of the tank, the side not facing the slide projector, the illuminated image of the tank was projected onto a sheet of tracing paper. This projected image was then recorded onto a computer using a 1MP JAI CCD camera. These images provided an integrated 2D qualitative view of the flow. For the experiments shown here, dye was added to the plume fluid and all images have been normalised by a background image with no dye or convective motion to further improve the contrast of the image.

4 Experimental results

4.1 Qualitative observations

Experiments were initiated in three distinct ways: (i) localised source first, (ii) distributed heating first, and (iii) both localised and distributed sources started simultaneously.

For case (i), shown in Figure 4, the localised source was switched on and after some time, a steady state was established where the volume flow rate of the plume at the interface balances the ventilation flow rate of the enclosure. Once this initial steady state was reached, and the change in interface height and temperature within the enclosure were negligible, the distributed source was switched on. The introduction of a distributed source introduced turbulence in the lower layer, with convective plumes rising from the floor that caused entrainment between the layers, disturbing the interface. For $\psi \lesssim 1$ the space still maintained a stratified interior. However, if $\psi \gtrsim 1$ the mixing between the layers was much more pronounced as in Figures 4e and 4f and the two-layer stratification within the enclosure was disrupted. Nevertheless, after a period of time a two-layer steady state could be reestablished. In case (ii), shown in Figure 5, once the system had reached its well-mixed steady state the localised source was switched on. Similar to case (i), a turbulent plume then formed above the source. As the plume rose and impacted on the top of the enclosure it was affected by the large-scale circulation already established in the space and initially there is an asymmetry as Figure 5a (cf. Figure 4a). Figure 6 shows snapshots from experiments of case (iii), where both sources were introduced instantaneously, and they were qualitatively similar to the case (i) experiments but with some transient mixing across the interface into the lower layer by the turbulent convection from the distributed source. Despite the very different time-dependent development of these flows with different initial conditions, the

ACCEPTED MANUSCRIPT

steady states in each case were the same, with no apparent hysteresis.

For all experiments the temperatures were monitored to determine when steady state was reached as in Figure 7 which shows the typical development of the temperature within the enclosure for case (iii). The ambient reservoir was monitored, the lower line of Figure 7, and seen to show negligible fluctuations in temperature. The development of two well-mixed regions separated by a stably stratified interface is clear. The upper dashed line of Figure 7 indicates a thermocouple located within the interface region. As the thermocouples were located on the inlet side of the tank, the lowest thermocouple, as represented by the lower dashed line of the Figure, is located within the region of the inlet itself, hence it detects the inflowing ambient fluid before it can fully mix with the lower layer. Similar increases in upper and lower layer temperatures were observed for larger values of $\psi \lesssim 1$ except for a period of time at the start of the experiments where the layers appeared mixed, with no discernible difference between the temperature of the layers.

Once steady state was established the traversing thermocouple recorded the temperature profile through the height of the enclosure. An example of such a profile can be seen in Figure 8. As in the transient temperature data, the profile displays two relatively well-mixed regions, separated by a stably stratified interface. Incoming ambient fluid, which is heated as it flows across the floor, accounts for the negative dimensionless temperatures at the bottom of the Figure. The interface height was determined from these profiles. The interface height h was defined as the point at which the temperature difference was 50% of the temperature difference between the layers, i.e.

$$h = z(T_l + 0.5\Delta T), \tag{20}$$

with $\Delta T = T_u - T_l$. The interface, as defined above, can be seen by the dash-dotted line in Figure 8.

4.2 Penetrative Convection - ϕ values

To see if penetrative convection, and hence entrainment between the layers, occurs the sensitivity of the model to various values of ϕ defined in (9) was examined. Figure 9 shows the comparison between experimental and theoretical results for a range of ϕ at fixed non-dimensional opening area β. The best agreement with the experimental data is for $\phi = 0$, suggesting that penetrative entrainment appears to be negligible over the full range of ψ shown where the enclosure remains stratified.

This conclusion is in qualitative agreement with the visualisations of the experiments shown in Figures 4, 5 and 6. If, in steady state, there was significant entrainment between the layers dyed fluid from the upper layer would be distributed in the lower layer, a feature not seen. This contradicts previous studies, for example Chenvidyakarn and Woods (2008) who found that a value of $\phi = 0.1$ gave a best fit to their experimental data. The main difference between the previous studies and the current experiments is the location of the

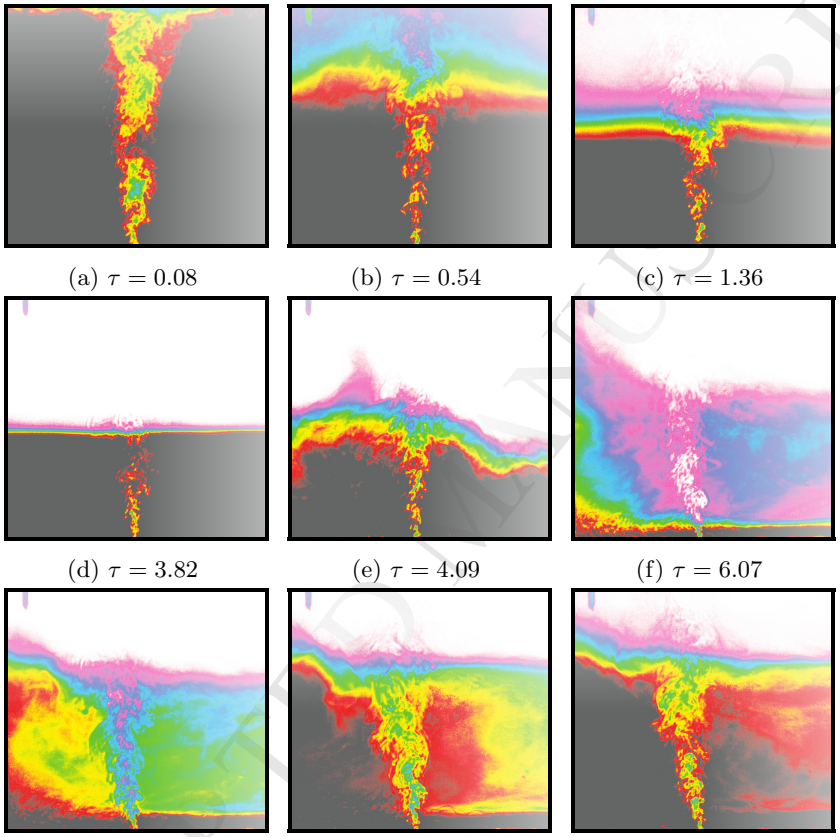

(a) $\tau = 0.08$ (b) $\tau = 0.54$ (c) $\tau = 1.36$

(d) $\tau = 3.82$ (e) $\tau = 4.09$ (f) $\tau = 6.07$

(g) $\tau = 6.55$ (h) $\tau = 7.09$ (i) $\tau = 7.64$

Figure 4: A series of images from an experiment where the buoyant plume fluid was dyed to aid visualisation. The images show the development of the flow at different non-dimensional times $\tau = \frac{t}{T_f}$. These images correspond to an experiment of case (i): the localised source was allowed to reach steady state prior to the distributed source being introduced with $\psi = 3.3$ and $T_f = 458.20$ s.

ACCEPTED MANUSCRIPT

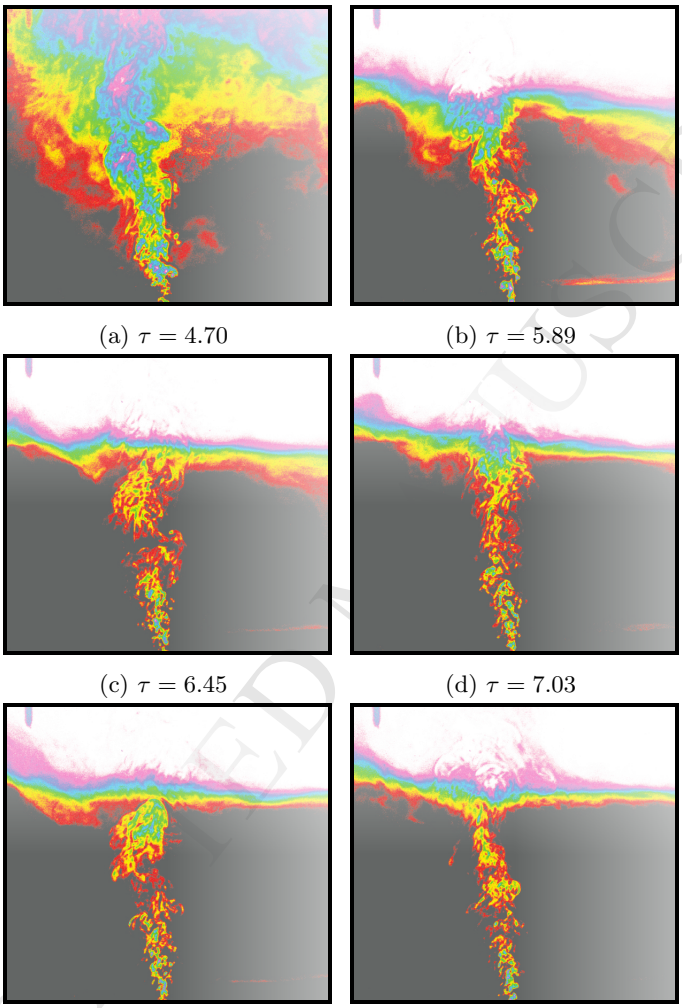

(a) $\tau = 4.70$ (b) $\tau = 5.89$

(c) $\tau = 6.45$ (d) $\tau = 7.03$

(e) $\tau = 7.60$ (f) $\tau = 8.17$

Figure 5: A series of images from an experiment where the buoyant plume fluid was dyed to aid visualisation. These images correspond to an experiment of case (ii): the distributed source was started initially and the space allowed to reach steady state prior to the localised source being introduced with $\psi = 3.3$ and $T_f = 436.05$ s.

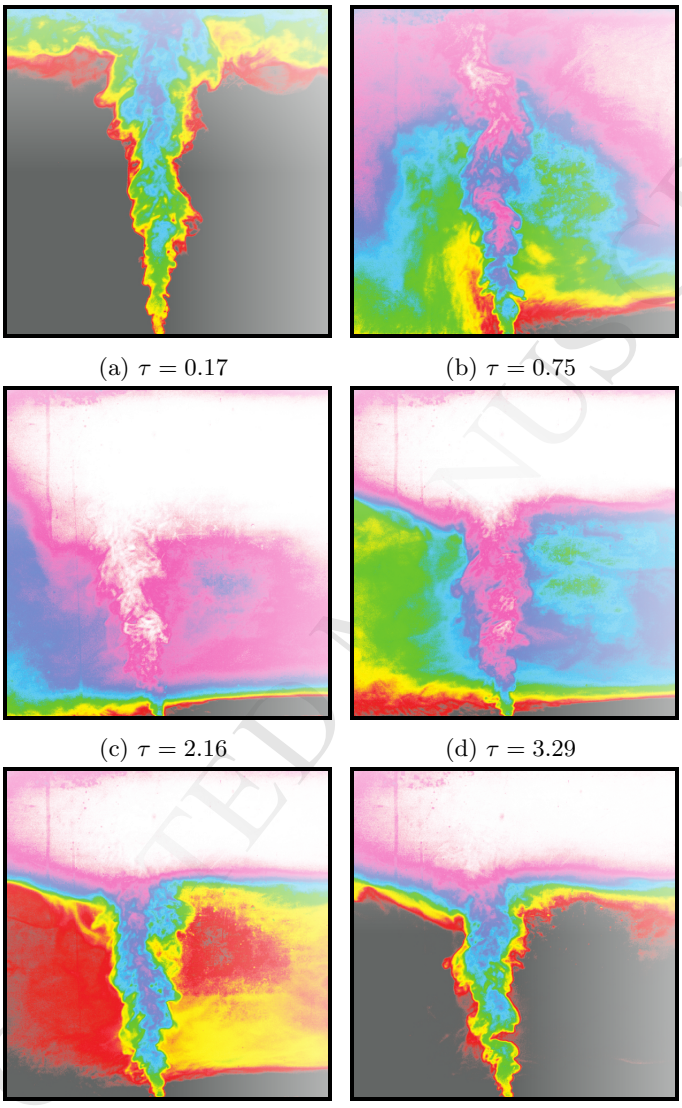

(a) $\tau = 0.17$ (b) $\tau = 0.75$

(c) $\tau = 2.16$ (d) $\tau = 3.29$

(e) $\tau = 4.72$ (f) $\tau = 6.54$

Figure 6: A series of images from an experiment where the buoyant plume fluid was dyed to aid visualisation. These images correspond to an experiment of case (iii): both the localised and distributed source were switched on at $t = 0$ with $\psi = 3.2$ and $T_f = 440.07$ s.

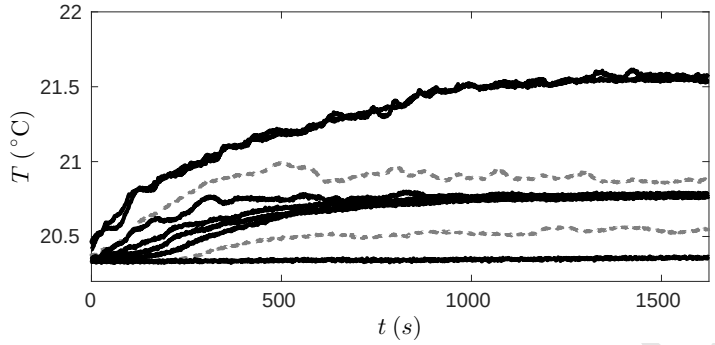

Figure 7: Transient temperatures from fixed thermocouples. Here $\beta = 0.63$, $\psi = 0.5$ and both sources were started instantaneously, i.e. it was case (iii). The upper dashed line displays a thermocouple which was in the interface region separating the layers and the lower dashed line displays a reading which was near the inlet. The thermocouple monitoring the external reservoir is shown by the lower line.

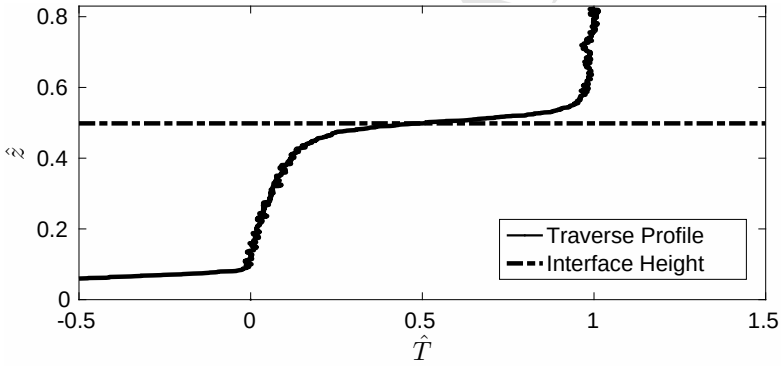

Figure 8: Temperature profile in steady state from the traversed thermocouple showing the choice of interface height. Here $\beta = 0.40$ and $\psi = 0.8$. The small fluctuations are the noise in the thermocouple. In the lower left you can see the sudden drop in temperature due to the relatively cool inflow of ambient fluid to replenish the fluid exhausted at the top of the enclosure. Due to this persistent cool inflow, the large-scale circulation within the space is maintained.

openings. In previous work horizontal openings were located in the upper and lower boundaries instead of the vertical openings in the side boundaries used here. Due to design constraints, wanting to maintain an enclosure that could easily have boundary conditions changed, horizontal openings were not possible in the current apparatus. Also, this change in opening position avoided vertical jets from the openings impinging directly on the interface. However, this orientation gave rise to a circulating cell in the lower layer which is a possible cause

ACCEPTED MANUSCRIPT

for the hindered mixing across the interface (see §5).

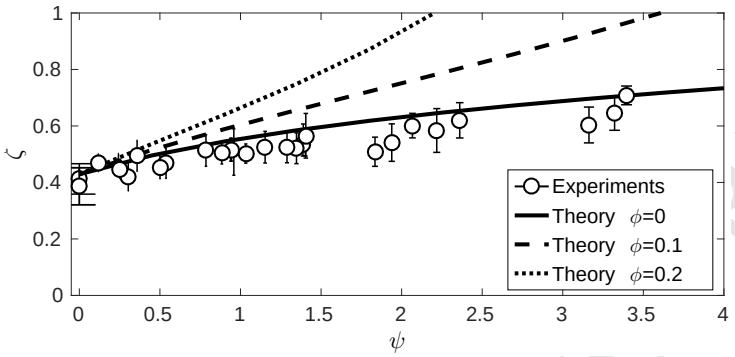

Figure 9: Steady-state interface results for $\beta = 0.40$, comparison with theory for varied values of penetrative convection parameter $\phi = 0, 0.1, 0.2$ is shown. Best agreement is found when penetrative convection is neglected, i.e. $\phi = 0$.

4.3 Interface Height

The variation of interface height with the dimensionless opening area β and ψ is shown in Figure 10, an increase in either ψ or β resulted in an increase in the interface height. Increasing β increases the ventilation flow rate (see (7)) while increasing ψ for fixed B_D results in an increase in total buoyancy within the system, which in turn also increases the ventilation flow rate. The increased flow rate through the enclosure forces the interface upwards allowing it to balance the flow rate in the plume. Although not explicitly examined experimentally, this is also true if the total buoyancy within the system $B_L + B_D$ is kept fixed and ψ is increased, as increasing ψ results in an increasing proportion of buoyancy within the lower layer which can drive a larger ventilation flow. This is to be expected as for $\psi \to \infty$ the room will transition to a well-mixed state with $\zeta = 1$. The theoretical model consistently over predicts the interface height when compared to the experimental results. We believe this consistent discrepancy is due to the slight ambiguity in defining the interface height as, in practice, there is always some finite interface thickness separating the upper and lower layers. The plume is only neutrally buoyant once it enters the upper layer and perhaps a more accurate definition of the interface, when compared to the theoretical model, would be the upper edge of the interfacial region which corresponds to the upper end of the error bars in Figures 9 and 10.

4.4 Buoyancy of the layers

Varying ψ also changes the buoyancy distribution in the system. Experimental results are shown in Figure 11 and compared with the theory. In these cases, increasing ψ makes both layers increasingly buoyant compared to the reduced

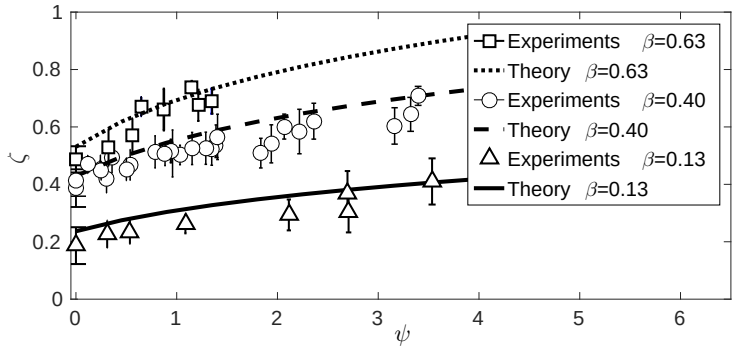

Figure 10: The non-dimensional steady-state interface height ζ with varying ψ and $\phi = 0$ for three different values of non-dimensional opening areas $\beta = 0.13, 0.40, 0.63$.

gravity of a localised source at the same interface height. This is a result of increasing the relative strength of the distributed source which not only adds buoyancy to the lower layer but also to the upper layer through entrainment into the plume. However, this is not the case if the total buoyancy $B_L + B_D$ is kept fixed within the enclosure. In such a situation the buoyancy within the lower layer would increase, and the upper layer buoyancy decrease, for increasing ψ.

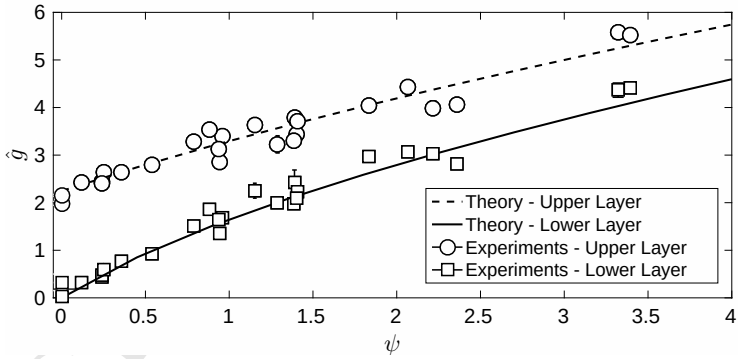

Figure 11: Non-dimensional reduced gravity of each layer with varying ψ, shown here for fixed non-dimensional opening area $\beta = 0.40$.

5 Model breakdown

For sufficiently large ψ and dimensionless opening areas β, which results in a larger ventilation flow rate through the space compared to smaller values of ψ and β, instead of a smooth transition to a well-mixed state, it was noted that the interface was no longer horizontal and the simple one-dimensional model

was no longer valid (see Figure 12). The model breakdown is investigated here.

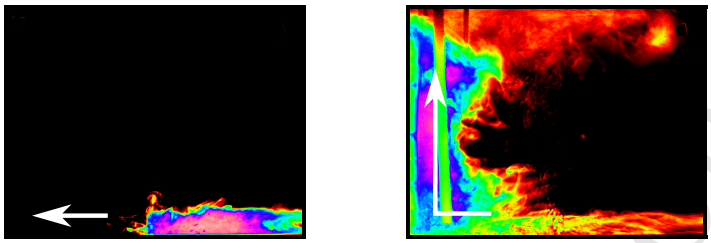

Figure 12: Images captured using DigiFlow showing the rising wall plume and short cut of the system at two different times, in this instance dye was added at the inlet to aid visualisation. The image on the left shows the incoming flow through the inlet and the image on the right shows the subsequent rise up the opposing boundary which penetrates the interface, not shown, and reaches the outlet. Here $\beta = 0.61$, $a_t = 50$ cm^2 and $a_b = 160$ cm^2, and $\psi \sim 4$.

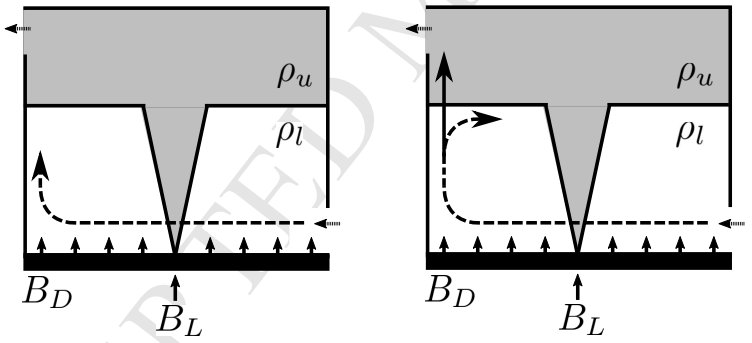

Figure 13: Qualitative flow pattern observed in the lower layer: left shows the initial circulation established by the inflow; right shows the subsequent flow determined by the interfacial Richardson number Ri, for $Ri < Ri_c$ significant mixing across the interface occurs (solid line) and for $Ri > Ri_c$ negligible mixing occurs and a single circulation cell is established (dashed line).

At these high ventilation rates, the dense flow through the inlet flows with sufficient speed across the floor to disrupt the convective motions from the distributed source. In this case, the flow from the inlet forces convective plumes from the distributed source to merge and rise at the downstream boundary. In order to understand the dynamics as the flow up the boundary reaches the interface, we choose to model the resulting flow up the far boundary as a line plume with buoyancy flux per unit depth B_D/D, where D is the depth of the

experimental tank ($D = 40$ cm for the experiments here). We also choose to neglect the wall stress in the subsequent flow up the boundary, where we are assuming the viscous boundary layer adjacent to the wall does not alter the bulk properties of the turbulent flow produced by the line plume. To check the significance of the inflow, experiments examining flow up the boundary with various inlet conditions were conducted. The velocity of the line plume u_w should be constant with height and scale on the buoyancy flux of the source $u_w \sim (B_D/D)^{1/3}$. This relation was verified by dyeing the inlet fluid and tracking the front position of the wall plume with time, an example of dyeing the inlet fluid and the subsequent flow up the boundary is shown in Figure 12. Figure 14 shows the front position data for a series of experiments with different source conditions and with the red line showing the scaling law for the plume velocity. For these experiments the lower opening was held fixed and spanned the whole depth of the tank to keep the flow across the distributed source, and the subsequent flow up the wall, two dimensional. The data suggest that the inlet conditions have minimal effect on the subsequent flow up the wall and merely act to establish the initial circulation. Therefore, modelling the flow from the distributed source as a line plume is reasonable.

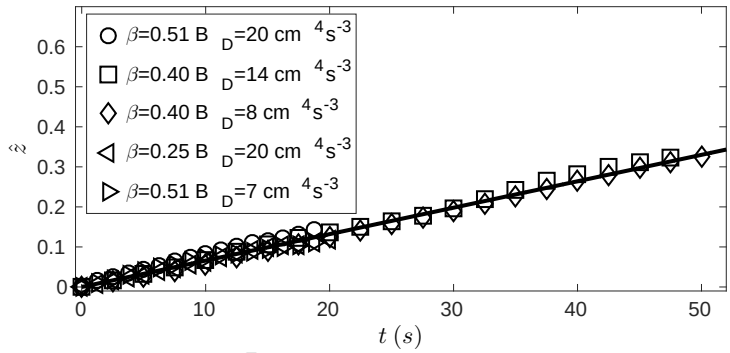

Figure 14: Wall plume dyed front position with time. Dye was added to the inlet when the system was in steady state to obtain a 'top-hat' velocity for the wall plume. The solid line shows the theoretical scaling for the velocity $u_w \sim (B_D/D)^{1/3}$.

Ching et al. (1993) examined the impact of a line plume on a density interface. They found a range of possible regimes depending on the interfacial Richardson number

$$\hat{Ri} = \frac{\Delta b l_d}{B_l^{2/3}}, \tag{21}$$

where Δb is the buoyancy jump across the interface, l_d is a characteristic length scale of the plume and B_l is the buoyancy flux per unit width of the line plume. For $\hat{Ri} > 5$ the penetration of the plume across the interface was found to be small, of the order of the interface thickness. When $1 < \hat{Ri} < 5$ there was

ACCEPTED MANUSCRIPT

evident mixing by the plume across the interface and for $\hat{Ri} < 1$ there was significant penetration across the interface and mixing by the plume.

The interfacial Richardson number can be examined for the steady state of the current system and hence whether or not the system can be expected to breakdown, with significant penetration of the wall plume across the interface. Modelling the merging convective plumes as a half line plume, and neglecting any wall stress, allows an interfacial Richardson number to be formed

$$Ri = \frac{\Delta g' h D^{2/3}}{B_D^{2/3}}, \tag{22}$$

where $\Delta g'$ is the reduced gravity of the buoyancy jump between the upper and lower layer. Examining the Richardson number it is possible to find when the two-layer stratification will breakdown, i.e. when $Ri < Ri_c$ with Ri_c some critical Richardson number. A qualitative view of the flow expected in the lower layer for different Ri values is shown in Figure 13. It should be noted that, as the Richardson number is based on the line plume properties, i.e. properties per unit depth, the penetration across the interface will occur even if the circulating flow is not uniform across the depth of the tank. In such an instance, a more complex three dimensional flow would be expected and the simplified model would not hold. Figure 15 shows the deviation between experimental and theoretical interface height with varied Richardson number. It is seen that interface height deviates from the theoretical value when $Ri \lesssim 5$. Comparison with Ching et al. (1993) is possible by noting that $l_d \simeq 0.16h$, and $\hat{Ri}_c \simeq 0.16 Ri_c$. Their data would suggest significant mixing across the interface when $\hat{Ri}_c \simeq 1$ or, in terms of the Richardson number used here, $Ri_c \sim 6$. This compares well with data from our current experiments.

It was also noted that for $Ri << Ri_c$ a completely different flow pattern was established. Given the location of the upper opening, it is possible for the flow in the lower layer to short cut the system and reach the upper opening. An example of a system short cut during an experiment is shown in Figure 12. In this regime the theoretical model is no longer valid, as entrainment into the plume is not the only way fluid can leave the lower layer. It was observed experimentally that the upper layer supplied by the plume fluid was substantially tilted in this flow regime with both upper and lower layer fluid leaving through the upper opening.

The critical Richardson number Ri_c puts a limit on the theoretical model derived in §2.1. However, there is still a rich range of ψ and β where the model is applicable, as seen in §4.

6 Application

As an example of a space containing both localised and distributed sources, consider a naturally-ventilated office with floor area of 20 m^2, a south facing window with area $A_g = 2$ m^2, and high and low level openings separated by a

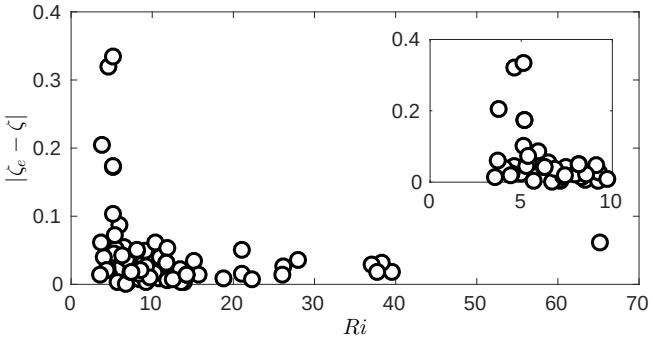

Figure 15: Absolute deviation between experimental (ζ_e) and theoretical (ζ) dimensionless interface height plotted against Richardson number. The model breaks down as $Ri \to 0$ with a critical Richardson number $Ri_c \simeq 5$.

vertical distance 3.5 m. The low level opening has an area 1 m^2 and the high level opening has an area 0.5 m^2. Assuming loss coefficients corresponding to sharp edged openings $c_t = c_b = 0.6$, the effective opening area of the space is $A^* = 1.25$ m^2.

Suppose the space contains an internal heat load from people and equipment of 17 Wm^{-2}, in line with values from CIBSE (2006), and that this gives rise to a localised heat source with heat flux $H_p = 340$ W. Driven by the localised source alone, there would be a warm upper layer at a height $h = 1.96$ m above the floor. The external temperature, and hence the temperature of the lower layer in this instance, is T_a, which, ignoring any other effects such as radiation, we assume would be perceived as comfortable by the majority of occupants. Now imagine that solar gains through the window drives a distributed heat source in the office. Let the heat flux of the distributed source be $H_f = 438.6$ W, where a typical value of transmitted solar radiation through a window from CIBSE (2006) has been taken, using the averaged solar data for London during August between 0830-1730, and where the floor is assumed to be of negligible thermal mass. Therefore, $\psi = 1.29$ for the given space. Using the theory of §2.1, we now find the room contains a warm, relative to the external temperature, upper and lower layer with an interface at height $h = 2.52$ m. Crucially, the temperature of the lower layer or 'occupied zone', relative to the ambient, will be $\Delta T_l = 1.78\,^\circ$C. Such a temperature anomaly, the difference between the lower layer temperature with and without distributed heating, could affect perceived thermal comfort by individuals. A temperature range of $T_i \pm 3\,^\circ$C, where T_i is the ideal indoor temperature for thermal comfort, would result in 10% Percentage People Dissatisfied (PPD) and is recommended for category II buildings (new buildings and renovations) (BS EN 15251,2007). The temperature change in the lower layer is not negligible compared to this temperature range and should be taken into consideration to avoid thermal discomfort.

This example illustrates the importance of solar gain through a glazed open-

ACCEPTED MANUSCRIPT

ing and how it could affect the thermal comfort of occupants. In the above calculation it was assumed that a large scale circulation was established in the lower layer, as seen in the small-scale experiments, and consequently any entrainment between the layers was ignored, i.e. $\phi = 0$. As an upper bound, we can include the entrainment term and investigate the temperature of the lower layer with $\phi = 0.2$. Doing so, a relative lower layer temperature $\Delta T_l = 2.10\,^{\circ}\mathrm{C}$ is found. As stated, this temperature could be taken as an upper bound for the temperature of the lower layer. In any practical application, it would be best practice to perform both calculations.

7 Conclusions

We have investigated the steady-state flows and stratification established in a naturally-ventilated enclosure containing both a distributed and localised source of buoyancy. The focus has been on an enclosure which allows displacement ventilation, i.e. lower and upper openings connect the space to an external ambient, as this makes a two-layer stratification possible.

A theoretical model has been constructed that extends the work of Chenvidyakarn and Woods (2008) to model enclosures that are naturally ventilated. In contrast to their experiments, penetrative convection was found to be negligible during steady state and appeared to only be a transient feature during the establishment of the ventilation flow and the stratification within the space. The lack of penetrative convection in the steady state appears to be a result of the background flow in the lower layer that is able to establish a large circulating mean flow that effectively switches off penetrative convection. The experiments conducted here demonstrate the importance of the background flow in naturally-ventilated spaces as has been demonstrated when investigating mixing caused by the inflow in the work of Hunt and Coffey (2010).

A number of experiments were carried out to validate the theoretical model and good agreement is found for a wide range of ψ and β. However, it is seen that the simple one-dimensional model breaks down for large ψ or high interface location ζ as shown in Figure 10. This breakdown occurs as $Ri \sim \left(\psi\zeta^2\right)^{-2/3}$ so increasing ψ or ζ destabilises the interface. Consequently, the critical value of ψ, the largest value of ψ that allows a two-layer stratification, is not a constant as suggested by Hunt et al. (2001b) but depends on the geometry of the enclosure in a complex manner. As Hunt et al. (2001b) was only a preliminary experimental study only a small range of opening areas were considered with $0.015 < \beta < 0.02$. This small range of opening sizes suggested that the critical value was a constant. The new experiments conducted in this paper, and the mathematical model, show that this is not the case with the stratification breaking down for $\psi < 6$ for large enough opening areas.

An example application has also been given and shows how important the inclusion of a distributed source is, even for relatively small ψ, and the implications it could have on thermal comfort. In practice, the value of ψ will vary between application and in particular the source of distributed heating. For

ACCEPTED MANUSCRIPT

distributed heating driven by solar gains an upper bound of ψ can be estimated by considering the peak transmitted solar radiation through a double-glazed window, which is ~ 600 W m^{-2}. Assuming a typical window to floor area ratio of 0.25 and an average localised heat gain of 17 W m^{-2} the estimate $\psi \sim 9$ is obtained for the upper bound. The actual value of ψ will be less than this value in reality, where cloud cover, shading, sun position, and other factors will decrease the transmitted solar radiation through the window. An alternative form of distributed heat source would be underfloor heating which has a maximum heat flux of 100 W m^{-2}. If we once again consider a localised heat gain of 17 W m^{-2} then $\psi \sim 6$ is found as the upper bound. These values indicate that, except for the extreme limits, the value of ψ in practice will likely fall in the range where the stratified model derived in this paper is valid.

Acknowledgments This work was supported by the Knowledge Transfer Network for Industrial Mathematics, and funded by the UK Engineering and Physical Sciences Research Council and by ARUP [EP/I501290/1]. We would also like to thank Dr Jake Hacker of ARUP, Prof Stuart Dalziel for his help in the laboratory and the technicians at DAMTP: David Page-Croft, Colin Hitch and John Milton. Finally, the authors would like to thank Prof. Gary Hunt and Dr Nigel Kaye for their helpful comments and suggestions.

References

Chenvidyakarn, T. and Woods, A. W. (2008). On underfloor air-conditioning of a room containing a distributed heat source and a localised heat source. *Energy and Buildings*, 40:1220–1227.

Ching, C. Y., Fernando, H. J. S., and Noh, Y. (1993). Interaction of a negatively buoyant line plume with a density interface. *Dynamics of Atmospheres and Oceans*, 19:367–388.

CIBSE (2006). *CIBSE, Guide A: Environmental design*. The Chartered Institution of Building Services Engineers, London.

Coomaraswamy, I. A. and Caulfield, C. P. (2011). Time-dependent ventilation flows driven by opposing wind and buoyancy. *Journal of Fluid Mechanics*, 672:33–59.

Deardorff, J. W., Willis, G. E., and Lilly, D. K. (1969). Laboratory investigation of non-steady penetrative convection. *Journal of Fluid Mechanics*, 35(01):7–31.

Fitzgerald, S. D. and Woods, A. W. (2007). Transient natural ventilation of a room with a distributed heat source. *Journal of Fluid Mechanics*, 591:21–42.

Gladstone, C. and Woods, A. W. (2001). On buoyancy-driven natural ventilation of a room with a heated floor. *Journal of Fluid Mechanics*, 441:293–314.

ACCEPTED MANUSCRIPT

Heidt, F. D. (1977). The growth of the mixed layer in a stratified fluid due to penetrative convection. *Boundary-Layer Meteorology*, 12(4):439–461.

Holford, J. M. and Hunt, G. R. (2001). The dependence of the discharge coefficient on density contrast. In *Proceedings of the 14th Australasian Fluid Mechanics Conference*, pages 123–126, Adelaide University, South Australia 5005, Australia.

Holford, J. M. and Hunt, G. R. (2003). Fundamental atrium design for natural ventilation. *Building and Environment*, 38(3):409–426.

Holford, J. M. and Woods, A. W. (2007). On the thermal buffering of naturally ventilated buildings through internal thermal mass. *Journal of Fluid Mechanics*, 580:329.

Hunt, G. R. and Coffey, C. J. (2010). Emptying boxes-classifying transient natural ventilation flows. *Journal of Fluid Mechanics*, 646:137–168.

Hunt, G. R., Cooper, P., and Linden, P. F. (2001a). Thermal stratification produced by plumes and jets in enclosed spaces. *Building and Environment*, 36(7):871–882.

Hunt, G. R., Holford, J. M., and Linden, P. F. (2001b). Natural ventilation by the competing effects of localised and distributed heat sources. In *Proceedings of the 14th Australasian Fluid Mechanics Conference*, pages 545–548, Adelaide University, South Australia 5005, Australia.

Hunt, G. R. and Kaye, N. G. (2001). Virtual origin correction for lazy turbulent plumes. *Journal of Fluid Mechanics*, 435:377–396.

Hunt, G. R. and Linden, P. F. (2001). Steady-state flows in an enclosure ventilated by buoyancy forces assisted by wind. *Journal of Fluid Mechanics*, 426:355–386.

Kaye, N. B. and Hunt, G. R. (2004). Time-dependent flows in an emptying filling box. *Journal of Fluid Mechanics*, 520:89–104.

Kaye, N. B. and Hunt, G. R. (2007). Heat source modelling and natural ventilation efficiency. *Building and Environment*, 42:1624–1631.

Lane-Serff, G. F. and Sandbach, S. D. (2012). Emptying non-adiabatic filling boxes: the effects of heat transfers on the fluid dynamics of natural ventilation. *Journal of Fluid Mechanics*, 701:386406.

Linden, P. F. (1999). The fluid mechanics of natural ventilation. *Annual Review of Fluid Mechanics*, 31:201–238.

Linden, P. F., Lane-Serff, G. F., and Smeed, D. A. (1990). Emptying filling boxes: The fluid mechanics of natural ventilation. *Journal of Fluid Mechanics*, 212:309–335.

ACCEPTED MANUSCRIPT

Menchaca-Brandan, M. A., Espinosa, F. A. D., and Glicksman, L. R. (2017). The influence of radiation heat transfer on the prediction of air flows in rooms under natural ventilation. *Energy and Buildings*, 138:530–538.

Morton, B. R., Taylor, G. I., and Turner, J. S. (1956). Turbulent gravitational convection from maintained and instantaneous sources. *Proceedings of the Royal Society A*, 234:1–23.

Partridge, J. L. and Linden, P. F. (2013). Validity of thermally-driven small-scale ventilated filling box models. *Experiments in Fluids*, 54(11):1–9.

Pérez-Lombard, L., Ortiz, J., and Pout, C. (2008). A review on buildings energy consumption information. *Energy and Buildings*, 40(3):394–398.

Wells, M. G., Griffiths, R. W., and Turner, J. S. (1999). Competition between distributed and localized buoyancy fluxes in a confined volume. *Journal of Fluid Mechanics*, 391:319–336.

ACCEPTED MANUSCRIPT

ACCEPTED MANUSCRIPT

Highlights

- New reduced order mathematical model presented to model the steady state of a naturally-ventilated enclosure containing a localised and a distributed source of buoyancy
- New, complimentary small-scale experiments conducted to assess the performance of the model
- Novel model constructed to predict when the reduced order model will breakdown
- Parameter ranges given for typical real world scenarios, highlighting when and how the model might be used.

ACCEPTED MANUSCRIPT